Sciortino A., Ferrante F., Mauro N., Buscarino G., Sciortino L., Giammona G., et al. (2021). Disclosing the emissive surface traps in green-emitting carbon nanodots.-
CARBON, 173, 454-461 [10.1016/j.carbon.2020.11.030].

DOI del contributo

https://dx.doi.org/10.1016/j.carbon.2020.11.030

Disclosing the emissive surface traps in green-emitting Carbon Nanodots

Alice Sciortino[a], *Francesco Ferrante*[a], *Nicolò Mauro*[b,c], *Gianpiero Buscarino*[a,d], *Luisa Sciortino*[a], *Gaetano Giammona*[b], *Marco Cannas*[a], *Dario Duca*[a], *Fabrizio Messina**[a,d]

[a] Dipartimento di Fisica e Chimica – Emilio Segrè, Università degli Studi di Palermo, Viale delle Scienze, Edificio 17, 90128 Palermo, Italy

[b] Dipartimento di Scienze e Tecnologie Biologiche, Chimiche e Farmaceutiche (STEBICEF) , Università degli Studi di Palermo, Via Archirafi 32, 90123 Palermo, Italy

[c] Fondazione Umberto Veronesi, Piazza Velasca 5, 20122 Milano, Italy.

[d] CHAB – ATeN Center, Università degli Studi di Palermo, Viale delle Scienze, Edificio 18, 90128 Palermo, Italy

Highlights

- Unravelling the microscopic origin of carbon nanodots fluorescence
- Synergy of chemical, physical experimental methods with computational techniques
- Surface carboxylic groups as the origin of carbon dot fluorescence

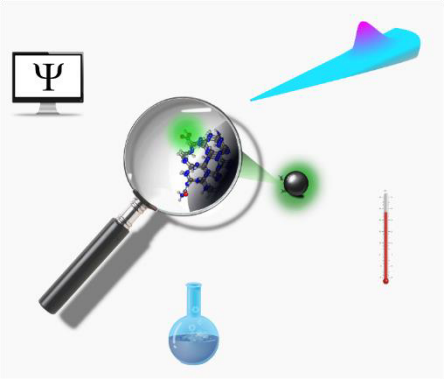

Graphical Abstract

*Corresponding Author. Email: **fabrizio.messina@unipa.it**

Abstract:

The bright photoluminescence of surface-functionalized carbon nanoparticles, known as carbon nanodots (CDs), has been studied for more than a decade because of its fundamental photo-physical interest and strong technological potential. However, the essential nature of the electronic states involved in their typical light emission remains very elusive. Here, we provide conclusive evidence that surface carboxylic moieties are the key to CD fluorescence. The synergy of nanosecond and femtosecond optical studies, cryogenic fluorescence, computational investigations and chemical engineering of a strategically chosen model CD system, allows to demonstrate that their visible-light transitions are due to the electron transfer from nitrogen atoms of the core to/from specific charge trap states strongly localized on –COOH surface groups. These results clarify a long-standing open problem in the photo-physics of carbon dots, and help to establish more solid foundations for the understanding of their optical response.

1. Introduction

Fluorescent carbon dots (CDs) have attracted considerable scientific attention thanks to their remarkable optical and functional characteristics, such as high emission efficiency in the visible range, low toxicity, high biocompatibility [1-4], ease of synthesis and versatile surface passivation [5-9]. Beginning from the very first work on CDs [10], and as later confirmed by countless studies, it was shown that the surface structure of these nanosystems is crucial to determine their optical properties. On one hand, a well passivated surface seems to be the key to activate efficient fluorescence [6,10] on the other hand, any modifications of the surface structure reflect into strong changes of the optical spectra [11]. Thus, the need of a properly functionalized surface to activate CD light emission is a cornerstone of our phenomenological understanding of CDs [11-12]. Nevertheless, neither the underlying reason is entirely understood, nor the specific role of different surface groups is clear. To explain the role of the surface, it was long hypothesized that CDs emission origins from the recombination of photoexcited charges which are temporarily trapped on certain surface sites. Although this idea has received a certain success [13], it has not been possible so far to identify the specific moieties which behave as surface traps. Here, we provide strong evidence that these traps can be identified as carboxylic groups.

Indeed, CD optical properties are highly debated and synthesis-dependent. Different authors hypothesize various types of electronic transitions: transitions within the carbogenic core [14], surface chromophores [15-17], molecular-like emission [18], or excitonic processes [19]. This variability is probably related to the many different types of CDs characterized by variable core and surface

structures and/or aggregation states (J-, H-aggregates) [20-21]. Despite of this, one can pinpoint some common features which are frequently encountered in the literature. In fact, the truly "archetypal" traits of CD optical spectra are two: broad and unstructured absorption bands covering the visible range, and a tunable fluorescence which, in the vast majority of cases, peaks in the green. In fact, although high emission quantum yield are often obtained for blue-emitting CDs, the reliability of these studies is often highly debated, considering the variety of blue emitting aromatic molecules that can be generated as side products from the synthesis, contaminating the true emission of CDs [18]. As for the structure, typical CDs have very high surface/volume ratios, due to the small size (<5 nm), and a disordered surface covered by a few types of polar functional groups: mostly -OH, -NH_2, -COOH, -$CONH_2$, which, in bottom-up synthesis routes, are left on the surface as residues of the reagents. Considering this, it makes sense to look for a common mechanism for the optical response of CDs even if the variability of their structures is quite large. In particular, it is reasonable to think that the emission directly involves one of these few simple moieties which are so ubiquitous on CD surfaces. On the other hand, high levels of nitrogen doping are often found essential to increase emission efficiency, but the underlying reasons are still unclear.

This study is founded on the synergy between experimental and theoretical studies of a carefully chosen model CD system. These dots were strategically selected because they display the archetypal optical response of CDs within a particularly small size (1.5 nm) and a simple structure, which makes them computationally feasible. This choice is very important in that it allows conducting a combined experimental-theoretical study on essentially the same system, without having to compare experimental data to unrealistic, excessively idealized theoretical models. Thereby, combining theoretical investigations with a comprehensive photophysical study (from femtosecond to nanosecond range) and using a well-controlled chemical passivation route, it is possible to clarify the typical photocycle of CDs. Our results directly highlight the electron transfer character of the electronic transition, while demonstrating the important role of nitrogen atoms in the core and key role of carboxylic groups as surface traps.

2. Materials & Methods

2.1 Synthesis, purification and functionalization of CDs: As previously reported [22] CDs have been obtained through a solvothermal synthesis in autoclave, mixing urea (6 g) and citric acid (3 g) in a DMF solution (30 mL) and heating to 160 °C for 4 h. When the solution cooled down, 60 mL of ethanol were added. After centrifugation procedures at 10000 rpm for 10 min and ethanol washing, a dark powder was collected and dispersed in water. Size exclusion chromatography (SEC)

was performed to purify the sample by using a glass column (100 cm length, 1.5 cm diameter) packed in turn with Sephadex G-25 (15 g), G-15 (15 g), and G-10 (30 g). Thereby, we selected a fraction of CDs with the most suitable characteristics for our experiment, as described in the main text. This sample was then subjected to surface functionalization via the following procedure. In a first step, the amino-PEG2000-alkyne (250 mg, 7.2×10^{19} chains) was dissolved in an aqueous solution of CDs (10 mL, 2 mg mL^{-1}, 3.4×10^{18} nanoparticles), the pH was set to 6.4, and EDC (24.92 mg, 0.13 mmol) and NHS (14.96 mg, 0.13 mmol) were added under stirring. The reaction was kept at pH 6.4 for 18 h and purified from the unreacted NH_2-PEG-CC and by-products through dialysis. A powder of P-CDs was obtained after freeze drying.

2.2 Atomic Force Microscopy (AFM): A drop of aqueous solution of either CDs or P-CDs (0.1 mg L^{-1}) was deposited on a mica substrate and then dried in vacuum. AFM measurements were carried out in air using a Bruker FAST-SCAN microscope equipped with a closed-loop scanner (X, Y, Z maximum scan regions: 35, 35, 3 μm, respectively). Scans were obtained in soft tapping mode using a FAST-SCAN-A probe with an apical radius of about 5 nm, and each image was obtained with a resolution comparable to the tip radius.

2.3 Transmission electron microscopy: The structure was characterized using a JEOL JEMS-2100 high-resolution transmission electron microscope (HRTEM) operating at 200 kV electron energy. Each sample was prepared in ultrapure water (1 mg L^{-1}) and deposited on a 400 μm mesh Cu grid covered by a holey amorphous carbon film, with a nominal thickness of 3 nm.

2.4 Infrared Absorption: IR measurements were acquired by a Bruker Alpha II spectrometer in transmission geometry (resolution: 4 cm^{-1}). Samples were prepared by dispersing CDs in KBr pellets, and the measurements were collected at room temperature under a nitrogen atmosphere to avoid artifacts.

2.5 Steady state absorption: Steady-state absorption measurements were carried out using a double beam spectrophotometer (JASCO V-560) in the 220−700 nm range in a 1 cm quartz cuvette.

2.6 Steady state emission: The emission spectra have been collected on diluted aqueous solutions of CDs and P-CDs (absorption<0.2 OD) by a JASCO FP-6500 spectrofluorometer in a 1 cm cuvette with a 3 nm resolution bandwidth.

2.7 Nanosecond time-resolved fluorescence: The emission decay kinetics were recorded by photoexciting the samples by 5 ns laser pulses of 0.1−0.3 mJ energy derived from a tunable laser (410-700 nm) consisting of an optical parametric oscillator (OPO) pumped by the third harmonic of a pulsed Q-switched Nd:YAG laser. The kinetic traces were detected by an intensified CCD camera which acquires the emission spectrum within a temporal window of 0.5 ns duration, with controlled

delays with respect to the laser pulse. The time resolution of the lifetime measurement was about 0.2−0.3 ns.

2.8 Cryogenic fluorescence measurements: Low-temperature fluorescence spectra were acquired in the nanosecond time-resolved fluorescence setup on SiO_2 samples (few ~mm^3 volume) containing a few ~mg/L of dispersed CDs, synthesized by a sol-gel method [23]. The measurements were conducted at T=10K on samples kept in high vacuum (10^{-6} mbar) within a continuous helium flow cryostat (OptistatCF-V, Oxford Instruments)**.**

2.9 Femtosecond transient absorption (TA): TA measurements were based on a 5 kHz Ti:sapphire femtosecond amplifier (Spectra Physics Solstice-Ace), which produces 75 fs pulses peaking at 800 nm (FWHM = 30 nm) at 350 mJ per pulse. This beam is split in two parts by a beam splitter (80%/20%) to generate the pump and the probe, respectively. To perform the experiments excited at 400 nm, on the pump arm, the 800 nm beam is frequency-doubled (type I phase-matching) by an ultrathin β-BBO crystal (250 mm) in order to create a 400 nm beam (20% efficiency), which is isolated from the fundamental by a Schott BG40 filter. This beam is chopped at 500 Hz and focused on the sample by a parabolic beam with f = 150 mm, while its polarization is controlled by a waveplate. To excite the sample at 266 nm, the 800 nm beam is frequency-tripled passing through a 400 nm-generating BBO, 800 nm waveplate, a retardation plate and, finally, into a 266 nm-generating BBO. After the generation, the beam passes through the same path of the 400 nm beam until it reaches the sample.

On the second arm, white light is generated focusing the 800 nm beam in a 1 mm quartz cuvette containing D_2O, generating a broadband pulse extending from 400 to 750 nm. The probe is focused on the sample by the same parabolic mirror used to focus the pump. The pump–probe delay is controlled by a motorized delay stage. The probe and the pump overlap within the sample, which continuously flows in a 200 mm thick flow cell upon the action of a peristaltic pump. The flow is regulated so that every pump pulse hits a fresh portion of the sample. After the sample, the probe beam is dispersed through a Brewster-angle silica prism and focused on the detector by a lens. The spectral resolution of this configuration is 3 nm. Pump and probe are synchronized using a camera detector system with 1024 pixels (Glaz Linescan-I) with single-shot capability. A typical signal is obtained by averaging 5000 pumped and 5000 unpumped spectra for each delay, and scanning over the pump–probe delay 10–20 times. The measurements were carried out under magic angle detection conditions. The data presented in the paper were subjected to standard correction procedures, which eliminate the effects of cross-phase modulation (XPM) and group velocity dispersion (GVD). The temporal resolution is about 70 fs for measurements pumped at 400 nm, 40 fs for measurements pumped at 266 nm.

2.10 Computational details:

The pristine CD model was tailored from bulk β-carbon nitride, β-C_3N_4, which crystallizes in the $P6_3/m$ spatial symmetry. In fact, this is the core crystalline structure expected at high N-doping levels, and confirmed by TEM analysis of our CDs (Figure S1). Nanosized β-C_3N_4, crystalline were synthesized and characterized by Yin and coworkers [24-25] and in some of our previous publications[26].

Full geometry optimization of CD and all modified CD systems were performed by using the Self Consistent Charge Density Functional Tight Binding approach at the full third order (SCC-DFTB3)[27] and the 3ob set of Slater-Koster parameter [28]. The derivative of Hubbard parameter needed for third order correction was H: -0.1857; C: -0.1492, N: -0.1535, O: -0.1575 and the damping exponent was setted to 4. These calculations were carried out by using the DFTB+ program [29].

The theoretical evaluation of dipole moment variation associated with the electron transition was performed by means of TDDFT, with the generalized gradient approximation exchange-correlation functional BLYP[30-32], joined with the correlation consistent polarized valence double zeta (cc-pvdz) basis set[33]. The gaussian 09 package [34] was used for these calculations. Incidentally, as regard the electron transition wavelengths in CD and modified CD, the trend obtained by considering the DFT-BLYP/cc-pvdz HOMO-LUMO difference is the same as the one resulted from DFTB calculations, being the presence of surface -COOH groups described as the only responsible of the adsorption in the visible region.

3. Results & Discussion

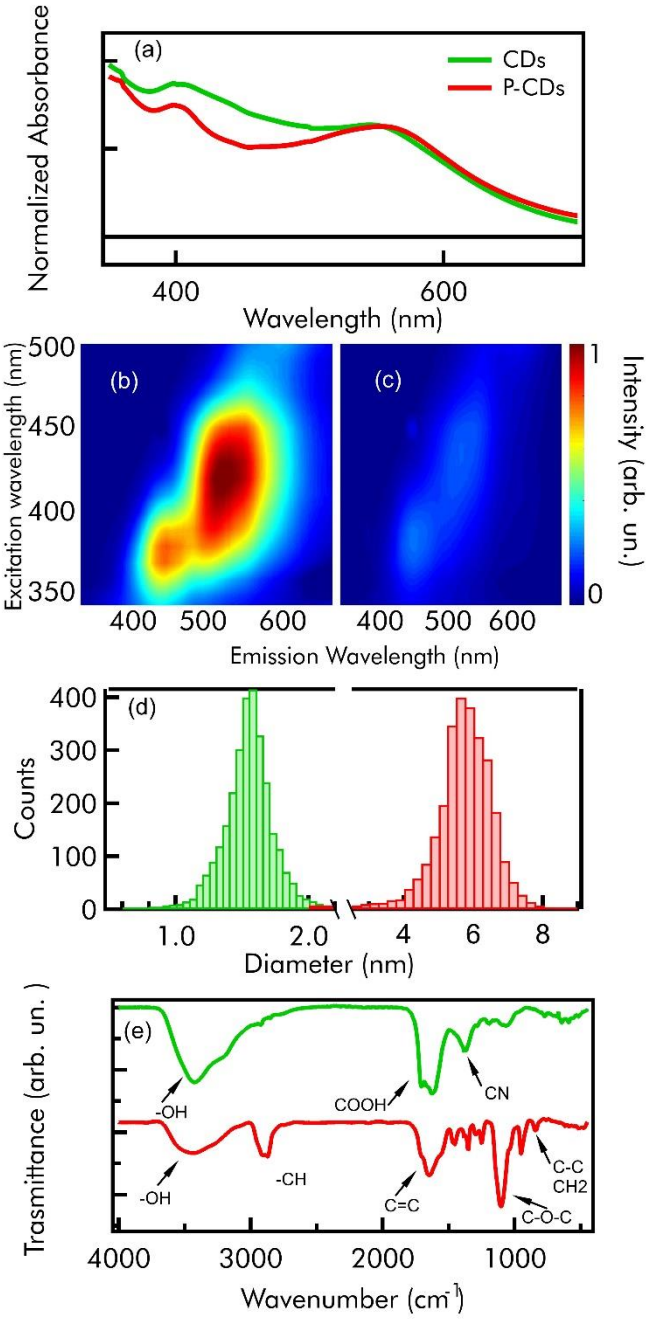

***Figure 1*:** Optical, morphological and structural characterization of the model CD system used in this work. Panel (a): Absorption spectra of an aqueous solution of CDs (green curve) and CDs after PEGylation, named P-CDs (red curve); Panel (b) excitation-emission 2D-plot of CDs and (c) of P-CDs; Panel (d) AFM size distribution of CDs (green histogram) and P-CDs (red histogram); Panel (e) Infrared spectra of CDs (green curve) and P-CDs (red curve).

CD fluorescence has been often related to the presence of nitrogen in the structure of the dot [35-36]. In fact, several works have found that a substantial degree of nitrogen doping is crucial to increase the emission efficiency above an acceptable threshold. For this reason, the CDs we used in this study were synthesized by a standard protocol that leads to green-emitting CDs with high nitrogen content and quantum efficiency >10%. Based on previous studies [22, 26], they are certainly expected to contain nitrogen not only in the surface, but also in the core structure. Indeed, the latter is expected to be in carbon nitride crystalline form [26] as confirmed by high-resolution transmission electron microscopy (Figure S1). From the crude CD sample synthesized as described in Methods section [22], we used size exclusion chromatography to isolate the CD sample which best fits the strategy of this study. These CDs have a simple spherical shape and particularly small size, narrowly distributed around 1.5 nm, as we see by atomic force microscopy (green histogram in Figure 1d and Figure S2). Their surface is covered by three common small functional groups, as shown by the infrared absorption spectrum in Figure 1e where the -hydroxyl (-OH, 3500 cm^{-1}), carboxylic (-COOH, 1710 cm^{-1}), and amide (-$CONH_2$, 1626 cm^{-1}) fingerprints are highlighted. These polar groups make these CDs very soluble in polar solvents and allow a controlled modification of the surface. The optical absorption spectrum (Figure 1a) covers all the visible range. Their steady-state emission (Figure 1b) can be efficiently excited from the near-UV to the visible, and displays the typical tunability of CDs (i.e. excitation-dependent peak position). However, the strongest fluorescence is emitted in the green, observed when exciting around 450 nm and peaking at 550 nm.

Starting from this, we demonstrate the key role of -COOH groups in the green-emitting electronic transition by observing the changes of the emission band induced by highly selective linking of amino-PEG_{2000}-alkyne chains to -COOH surface groups. To do so, the amino-PEG_{2000}-alkyne was initially dissolved in an aqueous solution of CDs. After the pH is adjusted to 6.4, 1-Ethyl-3-(3-dimethylaminopropyl)carbodiimide (EDC) and N-hydroxysuccinimide (NHS) were added to the solution which was stirred for 18 h. This allows the PEG chains to selectively link the carboxylic groups with high yield as confirmed by NMR data in Figure S4. These PEGylated CDs (named P-CDs) were finally purified from the unreacted PEG and from EDC and NHS by dialysis. As expected, the AFM data in Figure 1d show that the passivation of the surface causes an increase of the size of the dots from 1.5 nm to 6 nm, adding a soft corona which covers the CD cores, indicating that PEG-chains which are ≈2.1 nm long, are extended on the surface of the dots creating a brush-like configuration. However, the size distribution remains relatively narrow and single-peaked, demonstrating that the reaction is well-controlled and complete. Moreover, the appearance of new IR signals (Figure 1e), as C-C stretching and CH_2 rocking (841 cm^{-1}), C-O-C bending (1100 cm^{-1}), CH_2 rocking and twisting (954 cm^{-1}), C-H stretching (2880 cm^{-1}), and a decrease of COOH band intensity

in favour of C=C signal (1648 cm^{-1}) further confirm the occurrence of selective reaction at the COOH sites.

However, the most relevant consequence of PEGylation is the modification of the optical properties: green emission is strongly quenched, with the measured quantum yield decreasing from 13% to 1% (Figure 1c) leaving the absorption profile almost unaltered (Figure 1a). Even if the emission efficiency of green activity is very different, few variations are recorded in the emission lineshape and in the nanosecond decay kinetics, as shown in Figure S3. The strong drop in quantum yield with almost no changes in the nanosecond decay suggests that variations of the non-radiative rate decay occur in the sub-nanosecond time scale (as further confirmed below), while the recorded nanosecond lifetime is completely radiative. Therefore, covalent linking of PEG chains at the initial COOH sites opens up new sub-nanosecond decay channels quenching the emission, but the essential nature of the electronic transition is not altered.

Considering that PEGylation occurs through a highly selective reaction at the –COOH surface sites, these experimental results directly pinpoint the key role of carboxylic groups in the green emission of CDs. To support the interpretation of the experimental data, we performed computational investigations on several different model CD surface structures. A first study was performed on a "naked" CD model that, considering the experimental results (see Figure S1 and the literature [24]), was tailored from the bulk region of the carbon nitride structure and whose dangling bonds, originated in the fragment cutting, were saturated by hydrogen atoms. The obtained particle has $C_{65}N_{81}H_{79}$ stoichiometry and its largest linear size is ca. 1.2 nm. This is enough to discriminate surface from core regions and, very importantly, it is very close to the actual average size of the dots, leading to a realistic model. Then, chemical modifications on the surface were generated by substituting hydrogen atoms with the most common functional groups that can be found in CDs, namely carboxylic (-COOH), amidic (-$CONH_2$), aminic (-NH_2) and oxydrilic (-OH) groups. It was assumed that -COOH and -OH groups could be found on the CD surface as residues of the citric acid used for the synthesis, so they were attached to surface carbon atoms. On the other hand, -$CONH_2$ groups were attached to surface nitrogen atoms, being considered residues of the urea precursor. For the same reason, the extra -NH_2 group when included in the fragment model was bound to a surface C atom. The naked model fragment will be hereafter indicated simply by CD, while the surface-modified systems will be labelled as CD-nx, where n is the number of x groups anchored on the surface, namely -COOH, -$CONH_2$, -NH_2 and -OH in the order identified as c, a, n and o. All the models were subjected to full geometry optimization and investigated by the Self Consistent Charge Density Functional Tight Binding method at the third order (details in the Methods section).

As reported in Table 1 and Figure S5, the electronic gap of pristine CDs is very large (>7 eV), confirming that surface functionalization is crucial to activate optical transitions in the visible. In fact, we find that surface groups introduce electron states in-between the gap of pristine CD but, noticeably, among the various possibilities (c, a, n, o), only the presence of -COOH groups causes the appearance of absorption wavelengths (418-445 nm) which fall in the visible range (Table 1), strongly supporting the idea that COOH-induced states are those associated with the green emission occurring in CDs. These transitions are only slightly affected by the presence of any other groups which can be found simultaneously on the surface (compare for instance CD-1c1a, with one carboxylic and one amide group, with CD-1c). Furthermore, if more than one -COOH group is bound to the surface, an increased density of states is observed in the CD gap (see Figure S5), joined with only a slight variation of the lowest transition wavelength. This effect is likely due to minor distortions of the CD surface following the increasing number of COOH fragments. These distortions can affect the orientation of the COOH groups as well as their secondary interaction with the surface itself. The experimental absorption band, which is very broad (see Figure 1a), most likely comprises several of these transitions, consistently with the high inhomogeneity, and tunability, of the CD optical bands.

Table 1. Calculated wavelengths of the first vertical electronic transition in the pristine and modified CD models.

System	**λ (nm) / E(eV)**	**System**	**λ (nm) / E(eV)**
CD	161 / 7.67	CD-1c1a	422 / 2.94
CD-1c	429 / 2.89	CD-1n	159 / 7.75
CD-5c	418 / 2.96	CD-1o	161 / 7.68
CD-12c	445 / 2.79	CD-5PEG[a]	404 / 3.06
CD-1a	278 / 4.46	CD-12PEG[a]	402 / 3.08
CD-5a	286 / 4.33		

[a]Only a small portion of PEG is modelled, by means of a -NH-$(C_2H_4O)_3$-H group.

The calculated transitions energies, which should be considered only from a qualitative point of view, should be compared to the vertical electronic transition, that roughly corresponds to the peak of the excitation spectrum of the fluorescence. From the data in Figure S6, it is evident that the peak

of the photoluminescence excitation peak (420 nm) matches very well the simulated data for the CD-nc shown in Table 1, confirming the attribution to -COOH groups.

The theoretical investigations also disclose important details on the very nature of the electronic transition. We find that the electron excitation in all the investigated CDs can always be described as a core-to-surface electron density transfer, as witnessed by the difference between the electron density of the ground and excited states (Figure 2) and by the difference between the dipole moments of the two states above ($\Delta\mu$ is 8.22, 19.35 and 21.12 D for CD, CD-1c and CD-1a, respectively), calculated using time-dependent density functional theory (TDDFT). As a matter of fact, ancillary DFT calculations on selected systems show that the HOMO is localized almost exactly at the centre of the fragment core and, notably, on nitrogen centres which result to be crucial for the electronic transition, while the LUMO is localized near the surface in the CD case and on the functional groups on the CD-nx cases. This clearly demonstrates that, in order for the electronic transition to fall within the green spectrum, the nitrogen atoms in the core must interact with the -COOH surface traps. On one hand, this result clearly highlight the need of COOH functionalization to activate the electronic transition responsible of the green emission. On the other hand, the involvement of nitrogen in the optical transition provides an explanation to the frequent observation that nitrogen-doped CDs display strongly enhanced optical response [35-36]. Besides, the transfer of electronic charge towards the surface explains a series of well-known fingerprints of photo-excited CDs: high electron donor capability [37-39], strong interactions with solvents[40-41], ions[23] and molecules in solution[6], and enhanced sensitivity to H-bonds in the excited state[42-43].

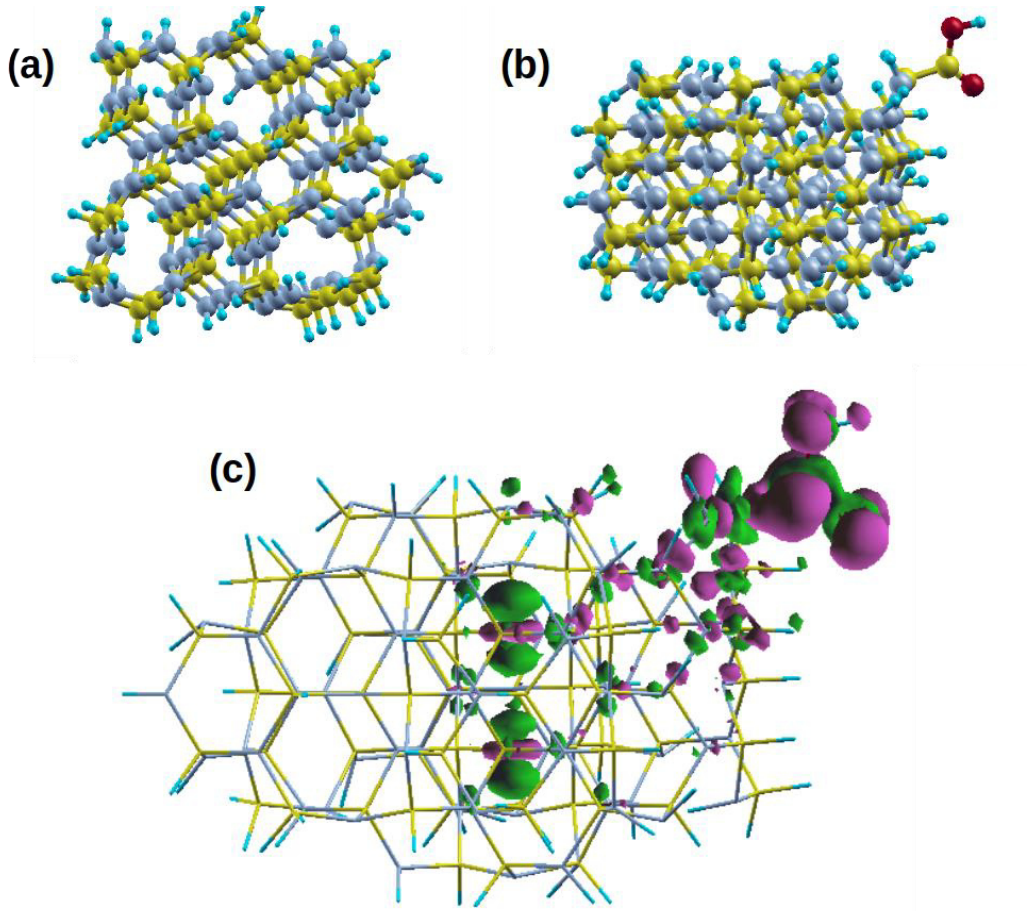

Figure 2: The optimized geometry of the $C_{65}N_{81}H_{79}$ (a) and $C_{65}N_{81}H_{78}$-COOH (b) CD particles, together with the representation of the TDDFT electron density difference isosurface of the latter system, at the |0.004| a.u. isovalue (c), calculated as $\Delta\rho(\mathbf{r}) = \rho_{exc}(\mathbf{r}) - \rho_{gs}(\mathbf{r})$. Color code is: yellow for C, pale blue for N, cyan for H and red for O

As a further method to probe the involvement of -COOH in the electronic transition, we performed fluorescence measurements at low temperature (10 K), still very rare on CDs. To this aim, the CDs were preliminarily embedded in a sol-gel monolith as previous reported [31]. While the room-temperature emission properties of solid-state CDs are almost identical to aqueous CDs (Figure S7), new features appear in the emission spectra at 10K exciting at long wavelengths, as shown in Figure 3. In fact, the low temperature causes a substantial narrowing of the band, revealing a vibronic progression associated to the green emission. The latter is clearly visible only at λ_{exc}>470 nm, that is in the red tail of the absorption range of CDs, probably because of a red-edge effect that causes a substantial decrease of the inhomogeneous broadening of the fluorescence band. The appearance of such a clear vibronic progression indicates a strong coupling with localized vibrations, that is another sign of an excited state which is highly localized on surface groups. The distance between the vibronic

peaks, as obtained by a fitting procedure, corresponds to an energy value of 120-140 meV (1050 ± 100 cm^{-1}) which matches the C-C vibration present in many carboxylic acids (e.g. 1053 cm^{-1} in citric acid[45]) confirming the attribution to COOH surface moieties. The range of variability of the vibrational frequencies is likely due to multiple possible configurations and local geometries of the COOH group on the surface of different dots, the properties of which are inhomogeneously distributed.

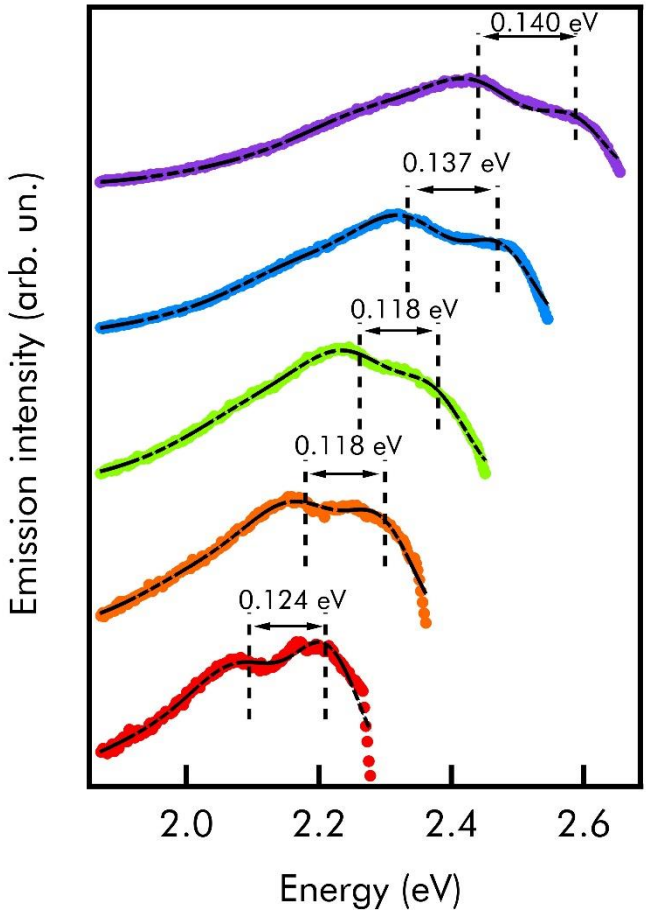

Figure 3: Emission spectra of CDs in a sol-gel matrix recorded at 10 K excited at 470 nm (purple line), 490 nm (blue line), 510 nm (green line), 530 nm (orange line) and 550 nm (red line) with the best fitting curves, obtained as explained in the SI.

After clarifying the fundamental nature of the green band, we further studied its photocycle performing femtosecond transient absorption (TA) measurements on both CDs and P-CDs at two different excitation wavelengths (400 nm and 266 nm) which are the two main peaks present in the fluorescence excitation spectrum (Figure S6). As illustrated in Figure S8, the TA spectra provide several observables which can be used to probe photo-induced dynamics. Here, we are mostly interested in two of them: the stimulated emission (SE) signal, which is equivalent to fluorescence

(albeit with inverted sign), and the excited-state absorption (ESA), which probes any transition to further excited energy levels which become accessible from the first excited state.

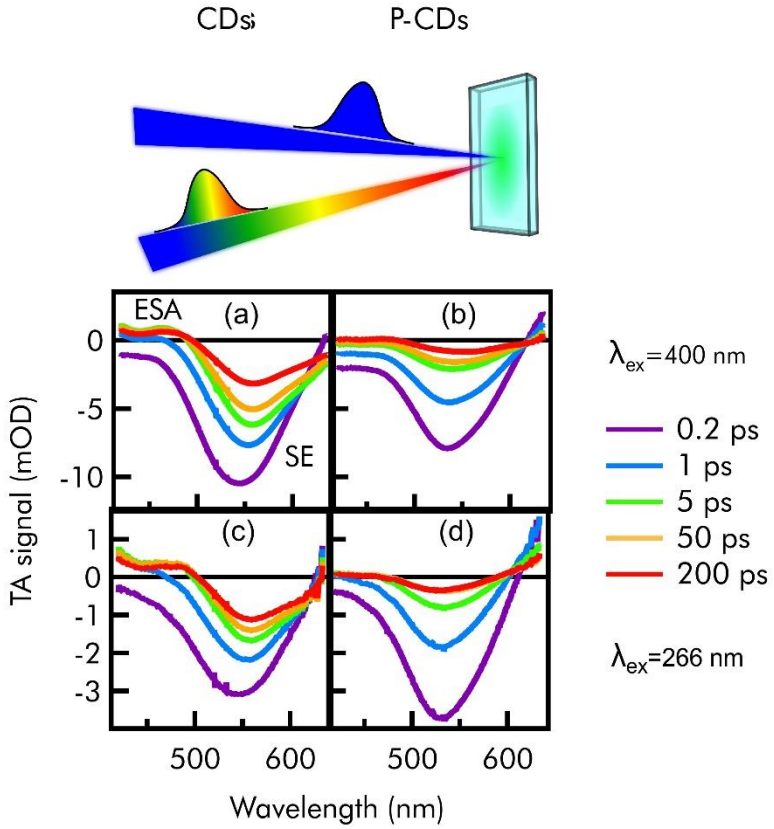

***Figure 4*:** Femtosecond transient absorption spectra of an aqueous solution of CDs (first column) pumped at 400 nm (panel a), and at 266 nm (panel c), and of P-CDs (second column) pumped at 400 nm (panel b) and at 266 nm (panel d), after different delays from photo-excitation.

At the earliest pump-probe delays, TA spectra of CDs excited at 400 nm (Figure 4a) display a SE peaking at 550 nm, which later redshifts and decays. The data at every delay are shown in Figure S9. In particular, during the first 5 ps the SE undergoes a progressive Stokes shift due to solvent relaxation around the photo-excited CD. This relaxation is bi-exponential, with time scales of 0.1 ps and 0.8 ps, as we found from a detailed analysis described in the SI (Figure S10 and Table S1). Such a strong excited-state interaction with surrounding solvent molecules is another consequence of the trapping of photo-induced charges on surface COOH sites, closely interacting with the surroundings. Together with the shift, the SE also undergoes intensity decay to 20-25% of its initial value within 200 ps (compare purple to red curve in Figure 4a). The extent of this decay is similar to the steady state QY (13%), directly confirming that the emission losses are mostly due to sub-nanosecond non-radiative events, as proposed above. At long times (red curve in Figure 4a) a small, but appreciable

ESA signal is observed around 480 nm in the TA spectra. From previous studies of CDs, the ESA is understood as the energy required to create a second exciton on the same dot after the first excitation [46], as also known for semiconductor quantum dots [47]. Here, the spectral position of the ESA is red-shifted with respect to the pump, which reveals that the electrostatic exciton-exciton interactions, in these CDs, are attractive.

Comparing now with P-CDs (Figure 4b, Figure S9, Figure S11 and Table S2), the overall shape of the TA signal is very similar, confirming that the essential nature of the emissive state excited at 400 nm is not changed by PEGylation. In fact, also theoretical calculations (Table 1) indicate that the vertical transition is hardly affected by PEGylation, showing only a small shift in presence of PEG-chains (compare e.g. CD-5c to CD-5PEG). However, in TA measurements, we do see some important changes in the dynamics, which explain the fluorescence quenching induced by PEGylation. The SE observed in P-CDs has the same shape as CDs but its redshift is less pronounced and slower (Figure S12): therefore, PEGylation effectively screens the CD from solvent interactions. Detailed data analysis shows that a significant portion of the solvation shift now occurs with a time scale as slow as 130 ps (Table S2 and Figure S11). Moreover, PEGylation amplifies the intensity decay of the fluorescence: in fact, Figure 4b directly shows that the SE signal drops to <10% within 200 ps. This finding explains the reduced emission efficiency of P-CDs and directly demonstrates our hypothesis that covalent bonding of PEG chains introduces new non-radiative channels responsible of the low QY of P-CDs. Non-radiative fluorescence decay often occurs through multi-phonon relaxation driven by specific hard vibrational modes [48]. So, we speculate that the additional non-radiative decay channels we find in P-CDs are driven by one of the several additional vibrational modes made available by PEG. From inspection of the FTIR spectrum (Figure 1e), the two most likely candidates are the very prominent C-O-C and C-H vibrations at 1100 cm^{-1} and C-H at 2880 cm^{-1}, respectively.

The last difference between CDs and P-CDs is the absence of the ESA at 480 nm in the latter, as better highlighted in Figure S13 where selected spectra from Figures 3a and 3b are compared. Considering that this signal probes bi-excitonic interactions, its disappearance after PEGylation suggests that the photo-excited charges, originally localized on COOH groups, get delocalized on the long PEG chains covalently attached to them, thus weakening exciton-exciton electrostatic interactions within the dot.

The photocycle excited at 266 nm (Figure 4c-4d and Figure S9), initiated from a higher energy state, display similar trends as exciting at 400 nm: each type of dot shows the same SE decay we see in the 400 nm-experiment and also in this case the solvation is slower for P-CDs than CDs. However, a detailed analysis reveals an additional difference between CDs and P-CDs. In the former, the TA spectral features of the green emission are already visible at “zero time” even when exciting at 266

nm (Figure S14); in contrast, the emission of P-CDs only shows up after a delay of about 400 fs (Figure S15 and Table S2), and the TA spectral fingerprints at "zero time" are entirely different. Therefore, the fundamental nature of the state initially excited at 266 nm is different in the two dots, likely because the intrinsic electronic states of PEG undergo a strong coupling with the high-energy states of CDs, significantly changing their nature.

4. Conclusions

In conclusion, we unravelled the identity of the surface charge traps responsible of the typical green fluorescence of carbon nanodots, which were recognized in the carboxylic groups.

Experiments and theoretical calculations conclusively agree on the character of the lowest-energy electronic transition of these nano-systems, which involves an electron transfer between the nitrogen atoms of the core and the carboxylic groups attached on the surface, both crucial for a bright emission. The fluorescence displays a series of specific fingerprints related to the involvement of carboxylic groups as surface traps: in particular, the selective passivation of carboxylic groups inhibits the emission modifying the sub-nanosecond relaxation dynamics by activating new non-radiative decay channels, and the excited state is strongly coupled with localized vibrational modes of carboxylic moieties.

Pinpointing the nature of the emissive charge traps in CDs solves one of the key open problems in the field. Such a result allows to model the fundamental electronic properties of these nanosystems within a simple and coherent frame, accounting for some of their well-known photophysical fingerprints, such as the strong response to the environment and electron donating properties.

References

1. Zhang, J. & Yu S.-H. Carbon dots: large-scale synthesis, sensing and bioimaging. *Materials Today,* **19**, 382-393 (2016).
2. Cao, l., Wang, X., Meziani, M.J., Lu, F., Wang, H., Luo, P. G., et al. Carbon dots for multiphoton bioimaging. *J. Am. Chem. Soc.,* **129,** 11318-11319 (2007).
3. Zuo. P., Lu, X., Sun, Z., Guo, Y. & He, H. A review on syntheses, properties, characterization and bioanalytical applications of fluorescent carbon dots. *Microchim. Acta,* **183**, 519-542 (2016).
4. Wang, J. & Qiu, J. A review of carbon dots in biological applications. *J. Mater. Sci.,* **51,** 4728-4738 (2016).
5. Zhu, H., Wang, X., Li, Y. Wang, Z., Yang, F., & Yang, X. Microwave synthesis of fluorescent

carbon nanoparticles with electrochemiluminescence properties. *Chem. Commun.*, 5118–5120, (2009).

6. Cayuela, A., Soriano, M.L. & Valcàrcel, M. Strong luminescence of Carbon Dots induced by acetone passivation: efficient sensor for a rapid analysis of two different pollutants. *Anal. Chim. Acta,* **804**, 246-251 (2013).
7. Li, X., Zhang, S., Kulinich, S. A., Liu, Y. & Zeng, H. Engineering surface states of carbon dots to achieve controllable luminescence for solid-luminescent composites and sensitive Be^{2+} detection. *Sci. Rep.,* **4**, 4976 (2015).
8. Hu, S., Chang, Q., Lin, K. & Yang, J. Tailoring surface charge distribution of carbon dots through heteroatoms for enhanced visible-light photocatalytic activity. *Carbon***, 105**, 484-489 (2016).
9. Dordevic, L., Arcudi, F. & Prato, M. Preparation, functionalization and characterization of engineered carbon nanodots. *Nat. Protoc.***, 14**, 2931-2953 (2019).
10. Sun, Y., Zhou, B., Lin, Y., Wang, W., Fernando, K. A. S. Pathak, P. et al. Quantum sized carbon dots for bright and colorful photoluminescence. *J. Am. Chem. Soc.*, **128**, 7756–7757 (2006).
11. Nguyen, H.A., Srivastava, I., Pan, D. & Gruebele, M. Unraveling the fluorescence mechanism of carbon dots with sub-single-particle resolution. *ACS Nano,* **14**, 6127-6137 (2020).
12. Li, L. & Dong, T. Photoluminescence tuning in carbon dots: surface passivation or/and functionalization, heteroatom doping. *J. Mater. Chem C.,* **6**, 7944-7970 (2018).
13. Xu, Y., Wu,M., Feng, X.-Z., Yin, X.-B., He, X.-W. & Zhang, Y.-K. Reduced carbon dots versus oxidized carbon dots: photo- and electrochemiluminescence investigations for selected applications. *Chem. Eur. J.,* **19**, 6282-6288 (2013).
14. Sun, M., Liang, C., Tian, Z., Ushakova, E.V., Li, D., Xing, G et al. Realization of the photostable intrinsic core emission from carbon dots through surface deoxidation by ultraviolet irradiation. *J. Phys. Chem. Lett.***, 11**, 3094-3100 (2019).
15. Nguyen, V., Si, J., Yan, L. & Hou, X. Direct demonstration of photoluminescence originated from surface functional groups in carbon nanodots. *Carbon,* **108**, 268-273 (2016).
16. Yang, H., Liu, Y., Guo, Z., Lei, B., Zhuang, J., Zhang, X et al. Hydrophobic carbon dot with blue dispersed emission and red aggregation-induced emission. *Nat. Comm.*,**10**, 1789 (2019).
17. Yuan, F., Wang, Y.-K., Sharma, G., Dong,Y., Zheng, X., Li, P. et al. Bright high-colour-purity deep-blue carbon dot light-emitting diodes via efficient edge amination. *Nat. Phot.,***14**, 171-176 (2020).

18. Longo, A. V., Sciortino, A., Cannas, M. & Messina F. UV photobleaching of carbon nanodots investigated by in situ optical methods. *Phys Chem Chem Phys,* **22**, 13398-13407 (2019)
19. Yuan, F., Yuan, T., Sui, L., Wang, Z., Xi, Z., Li, Y., et al. Engineering triangular carbon quantum dots with unprecedented narrow bandwidth emission for multicolored LEDs. *Nat. Comm.*, **9**, 2249 (2018).
20. Demchenko, A.P. & Dekaliuk, M. O. The origin of emissive states of carbon nanoparticles derived from ensemble-averaged and single-molecular studies. *Nanoscale,* **8,** 14057-14069 (2016).
21. Qu, D., Yang, D., Sun, Y., Wang, X. & Sun, Z. White emissive carbon dots actuated by the H-/J-Aggregates and Forster Resonance Energy Transfer. *J. Phys. Chem. Lett.,* **10**, 3849-3857 (2019).
22. Scialabba, C., Sciortino, A., Messina, F., Buscarino, G., Cannas, M., Roscigno, G., et al. Highly homogeneous biotinylated carbon nanodots: Red-Emitting nanoheaters as theranostic agents toward precision cancer medicine. *ACS Appl. Mater. Interfaces,* **11,** 19854-19866 (2019).
23. Sciortino, L., Messina, F., Buscarino, G., Agnello, S., Cannas, M & Gelardi, F. Nitrogen-doped carbon dots embedded in a SiO2 monolith fors solid-state fluorescent detection of Cu2+ ions. *J. Nanopart. Res.* **19**, (2017)
24. Yin, L.-W. Li, M.-S., Liu, Y.-X., Sui, J.-L. & Wang J.-M. Synthesis of beta carbon nitride nanosized crystal through mechanochemical reaction. *J. Phys.: Condens. Matter,* **15**, 309-314 (2003).
25. Yin, L.-W., Bando, Y., Li, M.-S., Liu, Y.-X. & Qi Y.-X. Unique Single-Crystalline Beta Carbon Nitride Nanorods *Adv. Mater.* **15,** 1840-1844 (2003).
26. Sciortino, A., Mauro, N., Buscarino, G., Sciortino, L., Popescu, R., Schneider, R., et al., F. β-C_3N_4 Nanocrystals: Carbon Dots with Extraordinary Morphological, Structural, and Optical Homogeneity. *Chem. Mater.*, **30**, 1695–1700 (2018).
27. Gaus, M., Cui, Q. & Elstner M. Extension of the Self-Consistent-Charge Density-Functional Tight-Binding Method (SCC-DFTB) *J. Chem. Theory Comput.* **7,** 931-948 (2011).
28. Gaus, M., Goez, A. & Elstner, M. Parametrization and Benchmark of DFTB3 for Organic Molecules *J. Chem. Theory Comput.* **9**, 338-354 (2013).
29. B. Hourahine, B. Aradi, V. Blum, F. Bonafé, A. Buccheri, C. Camacho, C. et al. DFTB+, a software package for efficient approximate density functional theory based atomistic simulations *J. Chem. Phys.* **152**, 124101 (2020).

30. Becke, A. D. Density-functional exchange-energy approximation with correct asymptotic behaviour. *Phys. Rev. A,* **38**, 3098-30100 (1988)
31. Lee,C., Yang,W. & Parr, R. G. Development of the Colle-Salvetti correlation-energy formula into a functional of the electron density. *Phys. Rev. B*, **37,** 785-789 (1988).
32. Miehlich, B., Savin, A., Stoll, H. & Preuss, H. Results obtained with the correlation energy density functionals of becke and lee, yang and parr. *Chem. Phys. Lett.*, **157,** 200-206 (1989).
33. Dunning Jr., T. H. *J. Chem. Phys.*, **90,** 1007-1023 (1989).
34. Frisch, M. J. et al. Gaussian 09 Revision D.01. Gaussian Inc. Wallingford CT (2009).
35. Yang, Z., Xu, M., Liu, Y., He, F., Gao, F., Su, Y., et al. Nitrogen-doped, carbon-rich, highly photoluminescent carbon dots from ammonium citrate. *Nanoscale,* **6**, 1890-1895 (2014).
36. Bhattacharyya, S., Ehrat, F. Urban, P., Teves, R., Wyrwich, R., Doblinger, M. et al. Effect of nitrogen atom positioning on the trade-off between emissive and photocatalytic properties of carbon dots. *Nat. Comm.,* **8**, 1401 (2017).
37. Wang, X., Cao, L., Lu, F., Meziani, M. J., Li, H., Qi, G., et al. Photoinduced electron transfers with carbon dots. *Chem. Comm*., **25**, 3774-3776 (2009).
38. Han, M., Zhu, S., Lu, S., Song, Y., Feng, T., Tao, S. et al. Recent progress on the photocatalysis of carbon dots: Classification, mechanism and applications. *Nanotoday*, **19**, 201-218 (2018).
39. Hu, S., Chang, Q., Lin, K & Yang, J. Tailoring surface charge distribution of carbon dots through heteroatoms for enhanced visible-light photocatalytic activity. *Carbon*, **105**, 484-489 (2016).
40. Pan, D., Zhang, J., Li, Z.;Wu, C., Yan X., & Wu, M. Observation of pH, solvent-, spin-, and excitation-dependent blue photoluminescence from carbon nanoparticles. *Chem. Commun*. **46**, 3681–3683 (2010).
41. Gharat P. M., Chethodil, J. M., Srivastava, A. P., Praseetha, P. K., Pal, H. & Choudhury, S. D. An insight into the molecular and surface state photoluminescence of carbon dots reveales through solvent-induced modulations in their excitation wavelength dependent emission properties. *Photochem. Photobiol. Sci.,***18,** 110-119 (2019).
42. Liu, H., Yang, J., Li,Z., Xiao, L., Aryee, A.A. Sun, Y., et al., X. Hydrogen-bond-induced emission of carbon dots for wash-free nucleus imaging. *Anal Chem.* **91**, 9259-9265 (2019).
43. Li, Q., Zhou,M., Yang,M., Yang, Q., Zhang, Z. & Shi, J. Induction of long-lived room temperature phosphorescence of carbon dots by water in hydrogen-bonded matrices. *Nat. Comm.,* **9**, 734 (2018).

44. Zhang, T., Zhu, J., Zhai, Y., Wang, H., Bai, X., Dong, B., et al. A novel mechanism for red emission carbon dots: hydrogen bond dominated molecular states emission. *Nanoscale*, **9**, 13042-13051 (2017).
45. Bichara, L. C., Lanùs, H. E., Ferrer, E. G., Gramajo, M.B. & Brandàn, A. Vibrational study and force field on the citric acid dimer based on the SQM methodology. *Adv. Phys. Chem,* 347072 (2011).
46. Sciortino, A., Gazzetto, M., Buscarino, G., Popescu, R., Schneider, R., Giammona, G., et al. Disentangling size effects and spectral inhomogeneity in carbon nanodots by ultrafast dynamical hole-burning. *Nanoscale*, **10**, 15317–15323 (2018)
47. Klimov, V. I. Spectral and dynamical properties of multiexcitons in semiconductor nanocrystals. *Annu. Rev. Phys. Chem.* **58**, 635-673 (2007).
48. Yu, D., Ballato, J. & Riman, R. E. The temperature-dependence of multiphonon relaxation of rare-earth ions in solid state hosts. *J. Phys Chem C*, **120**, 9958-9964 (2016).

Acknowledgements

This work was supported by the "L'Oréal Italia Per le Donne e la Scienza" Program. The authors thank G. Napoli for technical assistance in low temperature measurements. The authors thank the LABaM group at University of Palermo for support and stimulating discussions.

Credit author statement

A.S., F.F, D.D. and F.M. designed the study and wrote the manuscript in consultation with all the other authors. A.S. and F.M. performed the optical characterization. A.S, M.C. and F.M. developed the interpretation of the optical data. F.F. and D.D. performed the computational studies. N.M. and G.G. contributed with the synthesis, the chemical passivation and the IR measurements. L.S. and F.M. carried out the cryogenic measurements. G.B. carried out the morphological characterization.

Competing interests

The authors declare no competing interests